

Journal of Materials Chemistry B

Accepted Manuscript



This is an *Accepted Manuscript*, which has been through the Royal Society of Chemistry peer review process and has been accepted for publication.

Accepted Manuscripts are published online shortly after acceptance, before technical editing, formatting and proof reading. Using this free service, authors can make their results available to the community, in citable form, before we publish the edited article. We will replace this *Accepted Manuscript* with the edited and formatted *Advance Article* as soon as it is available.

You can find more information about *Accepted Manuscripts* in the [Information for Authors](#).

Please note that technical editing may introduce minor changes to the text and/or graphics, which may alter content. The journal's standard [Terms & Conditions](#) and the [Ethical guidelines](#) still apply. In no event shall the Royal Society of Chemistry be held responsible for any errors or omissions in this *Accepted Manuscript* or any consequences arising from the use of any information it contains.

Aqueous synthesis of polyhedral “brick-like” iron oxide nanoparticles for hyperthermia and T_2 MRI contrast enhancement†

Cite this: DOI: 10.1039/x0xx00000x

Received 00th January 201x,
Accepted 00th January 201x

DOI: 10.1039/x0xx00000x

www.rsc.org/

Matthew Worden^a, Michael A. Bruckman^b, Min-Ho Kim^d, Nicole F. Steinmetz^{bc}, James M. Kikkawa^c, Catherine LaSpina^a and Torsten Hegmann^{*af}

A low temperature, aqueous synthesis of polyhedral iron oxide nanoparticles (IONPs) is presented. The modification of the co-precipitation hydrolysis method with Triton X surfactants results in the formation of crystalline polyhedral particles. The particles are herein termed iron oxide “nanobricks” (IONBs) as the variety of particles made are all variations on a simple “brick-like” rhombohedral shape as evaluated by TEM. These IONBs can be easily coated with hydrophilic silane ligands, allowing them to be dispersed in aqueous media. The dispersed particles are investigated for potential applications as hyperthermia and T_2 MRI contrast agents. The results demonstrate that the IONBs perform better than comparable spherical IONPs in both applications, and show r_2 values amongst the highest for iron oxide based materials reported in the literature.

Introduction

Iron oxide nanoparticles (IONPs, composed of either magnetite, Fe_3O_4 , or maghemite, $\gamma\text{-Fe}_2\text{O}_3$) have been used for several decades in many disparate fields, including environmental remediation¹, energy storage,² and catalysis³. In addition, an increasingly prominent area of investigation is in biomedical applications, including drug delivery, MRI contrast enhancement, and magnetic hyperthermia.⁴ The effects of the surface chemistry of functionalized IONPs on such biological and medical applications are fairly well established, as demonstrated in various reviews on the topic.⁴ A frequently overlooked aspect of these reviews, however, is the effect that particle morphology may have on these applications. This is unsurprising, as the vast majority of publications deal with very similar core shapes and sizes, almost certainly because most synthetic methods for creating IONPs yield particles of similar morphology (*i.e.* quasi-spheres in the range of a few to tens of nanometers).

In terms of aqueous syntheses, one of the oldest and most widely used methods is the co-precipitation method by Massart, in which a mixture of Fe^{2+} and Fe^{3+} salts are hydrolyzed under basic conditions in water, yielding roughly spherical IONPs.⁵ A more recent method by Yathindranath *et al.* accomplishes the same by reducing $\text{Fe}(\text{acac})_3$ with NaBH_4 in basic conditions at room temperature.⁶ Both of these methods allow for simple

coating of the resulting particles by the addition of hydrophilic functionalizing agents such as siloxanes and certain polymers.

In general, non-aqueous methods offer a greater degree of control over particle size and homogeneity. One of the earliest and most widely cited examples, reported by Sun *et al.*, involves $\text{Fe}(\text{acac})_3$ reacted at 265 °C in a mixture of phenyl ether, an alcohol, oleic acid, and oleylamine, with the latter two compounds acting as *in situ* stabilizing ligands.⁷ This method produces highly monodisperse, pure magnetite particles below 20 nm in size. The basic strategy of thermal decomposition of an iron precursor in a high boiling point solvent to create spherical IONPs has been repeated and modified a number of times.⁸ Recently, further modifications on this method have allowed for the creation of non-spherical particles. Lee *et al.* developed a thermal decomposition reaction of $\text{Fe}(\text{CO})_5$ in a mixture of DMF and various imidazolium-based ionic liquids to create $\gamma\text{-Fe}_2\text{O}_3$ NPs of various shapes.⁹ Depending on the reaction conditions and specific ionic liquid used the particles could be short “bars” about 50 nm in length, or longer “wires” several hundred nanometers in size. Yang *et al.* synthesized magnetite “nanocubes” by heating $\text{Fe}(\text{acac})_3$ in a mixture of oleic acid, oleylamine, 1,2-hexanediol and benzyl ether. This method allowed them to obtain monodisperse nanocubes as small as 6.5 nm.¹⁰ Guardia *et al.* demonstrated a somewhat tighter control on the size and distribution of nanocubes at a lower temperature by replacing oleic acid with decanoic acid.¹¹ Palchudhury *et al.* performed a relatively low temperature (150

°C) decomposition reaction of iron oleate to create what they termed “iron oxide nanowhiskers” approximately 50 nm long.¹² However, these nanowhiskers are poorly crystalized and must undergo post-synthesis calcination. Bao *et al.* demonstrated a synthesis of iron oxide nanorods that allowed for some degree of control over size and aspect ratio.¹³ A recent publication by Mitra *et al.* showed that changes in heating rate during a synthesis that normally results in spherical particles resulted in octahedral particles.¹⁴ The authors suggested that the lower surface anisotropy of octahedra, as compared with that of spheres, causes the differences in certain magnetic properties between these types of particles.

In almost all cases mentioned above, non-spherical IONPs have been made at high temperature, non-aqueous conditions and often with the use of toxic solvents, which does not directly result in particles that are dispersible in aqueous media. Post-synthesis ligand exchange procedures must be conducted to allow for the particles to be dispersed in biologically relevant media.¹⁵⁻¹⁶ In order to avoid such extra steps, not to mention the additional costs associated with high temperature methods and organic solvents, an aqueous method that allows for the control and alteration of the IONP morphology and permits simple functionalization with hydrophilic ligands is highly desirable.

In a recent publication we reported some first steps towards this goal. An aqueous reduction/hydrolysis of iron(III) chloride with sodium borohydride was conducted in the presence of Triton X100, a surfactant that when mixed with water behaves as a lyotropic liquid crystal (LLC).¹⁷ This synthesis resulted in the formation of 2D sheets composed of a mixture of crystalline iron and iron oxide. These sheets, while only a few nanometers thick, were much larger in other dimensions (hundreds of nanometers) and the total size was difficult to control. Herein we report a modification of that technique which offers more precise control of particles fully “nano” in all dimensions, composed entirely of a single phase of iron oxide. A mixture of iron chloride precursors was hydrolyzed in water with sodium hydroxide in the presence of a surfactant (Triton X45 or Triton X100). The resulting iron oxide particles are a mixture of anisometric polyhedral particles with “brick-like” shapes of varying aspect ratios. The precise ratio between particle types depends on the reaction conditions. The use of Triton X45 – which can form a lamellar phase LLC in water¹⁸ – allows for the formation of predominantly rectangular and rhombohedral “nanobricks” labelled **IONBsX45**. The synthesis with Triton X100 - which, in a 50% mixture with water, forms a hexagonal phase LLC¹⁹ – allows for the formation of smaller cubic and rhombohedral particles, labelled **IONBsX100**. These particles can be easily functionalized with siloxane molecules, allowing for dispersal in aqueous media and thus potential use in biomedical applications.

Two such applications, as noted above, are in the areas of magnetic hyperthermia and MRI contrast enhancement. The former technique involves exposing magnetic particles (either ferro- or superparamagnetic, depending on the material) to an external AC magnetic field, the energy of which is converted to heat in the particles through Brownian and Neel relaxation

mechanisms. A number of publications have looked at IONPs in hyperthermia treatment of cancer and tumor cells, as well as infectious agents such as bacteria, both *in vivo* and *in vitro*, with promising results.²⁰ Particle size and shape can play important roles in the overall efficiency of this process.²¹ With this in mind we compared both types of NPs, functionalized with a hydrophilic siloxane, with spherical IONPs coated with the same siloxane. The results demonstrate that both kinds of anisometric NPs are significantly more efficient than comparable spherical IONPs for hyperthermia applications.

The superparamagnetic behavior of IONPs allow them to be used as T_2 (negative contrast) agents in MRI diagnostics. Indeed a number of commercial IONP-based contrast agents have been clinically available for many years.²² All of these are spherical particles, however. As with the properties associated with hyperthermia, particle shape can affect the efficiency of IONPs as MRI contrast agents.²³ We analyzed the same particle systems mentioned above, at varying magnetic field strengths, for their efficacy as T_2 contrast agents. Our anisometric NPs provided both higher r_2 relaxivity values as well as higher r_2/r_1 ratios than comparable spherical NPs, and in fact performed similarly to the most effective commercially available particles currently on market.

Results and Discussion

Synthesis of IONBsX45 and IONBsX100

In a typical experiment FeCl_3 (2 mmol) and $\text{FeCl}_2 \cdot 4\text{H}_2\text{O}$ (1 mmol) were dissolved in 20 mL of degassed water and added to a 3 neck round bottom flask under nitrogen. This reaction vessel was heated to 50 °C, at which point 25 mL of degassed Triton X surfactant (either X45 or X100, depending on the experiment) was added and mechanically stirred at 100 rpm to ensure that a homogeneous mixture was formed. The vessel was then cooled to 35 °C in the case of X45, and 30 °C in the case of X100. NaOH (30 mmol) was then dissolved in 5 mL degassed water and added to the above mixture under nitrogen and 100 rpm mechanical stirring. The thick, yellow mixture quickly turned black as the NaOH was mixed in. The reaction was left to mix for 1 hour. The black product was washed with warm water and centrifuged at 10,000 rpm several times to isolate it from the surfactant, then dried under nitrogen and stored as a powder under ambient conditions.

Synthesis of S-IONBsX45 and S-IONBsX100

Silanized IONBs (**S-IONBs**) were synthesized following a modification of the above procedure. One hour after the addition of the NaOH solution, 15 mL of EDTS (45% in water) was added *via* syringe directly into the reaction vessel. The reaction was left to mix for 12 hours. The product was isolated *via* multiple washings with a water/ethanol mixture and centrifugation at 10,000 rpm, and then dried under nitrogen. The black powder could then be stored under ambient conditions or re-dispersed in aqueous solution for further use.

Evaluation of particle morphology and crystallinity

Figure 1 shows the powder X-ray diffraction (XRD) patterns of bare **IONBsX100** and **IONBsX45**. The indexed patterns match closely to that of bulk magnetite (ICDD reference code 01-089-0691) as well as maghemite.

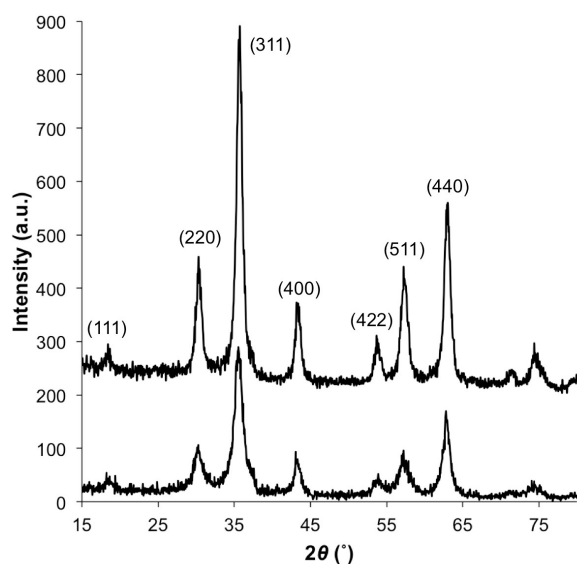


Figure 1: Powder XRD patterns for **IONBsX100** (top) and **IONBsX45** (bottom). Peaks have been indexed to match that of bulk magnetite.

The most important question concerned whether the addition of the surfactants could in fact allow for some measure of control over particle shape. TEM imaging was thus used on the bare **IONBsX45** and **IONBsX100** in order to answer this question. Figures 2A-D shows representative high-resolution (HR)-TEM images of **IONBsX45**. The particles are composed primarily of rectangular and rhombohedral shapes, with a distribution of sizes of approximately 15 +/- 10 nm, and with varying aspect ratios between edge lengths therein. An average d -spacing of approximately 4.9 Å for the visible lattice fringes was determined *via* analysis with ImageJ® software (Figure 2D), and is consistent with the d -spacing (4.842 Å) associated with the (111) lattice plane of magnetite.

Figures 3A-D shows representative HR-TEM images of **IONBsX100**. These particles differ noticeably from those made with X45. They include primarily rhombohedral shapes with edges of similar lengths of approximately 10 +/- 5 nm. The longer rectangular particles seen with X45, in which perpendicular sides have varying aspect ratios, are not seen with X100. An average d -spacing of approximately 4.8 Å was determined (Figure 3D), again close to that of the d -spacing associated with the (111) lattice plane of magnetite.

Further evaluation of particle morphology is shown in Figure 4, which compares TEM images of various particles with 3D representations (shown adjacent to the relevant TEM images) of shapes to which they most likely conform. The figure starts from a rhombohedral “brick”. Figure 4A shows the face of this rhombohedron, with B (from X45) and C (from X100) showing representative particles with this shape under

TEM; Figure 4D shows a larger shape in which one of the pair of edges is elongated to form a parallelepiped (3D parallelogram), with E and F showing representative TEM images of this shape from **IONBsX45**; Figure 4G shows the same shape as D as viewed along the long edge, resulting in a rectangular shape, with H and I showing representative TEM images of this shape from **IONBsX45**.

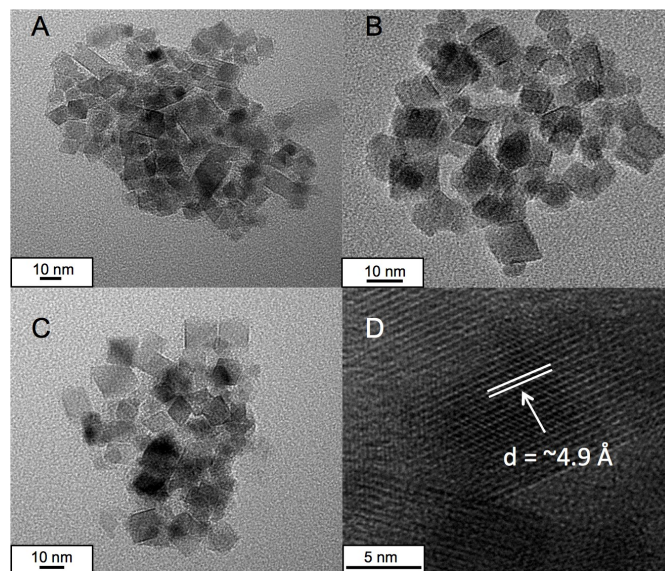


Figure 2: TEM images of **IONBsX45**.

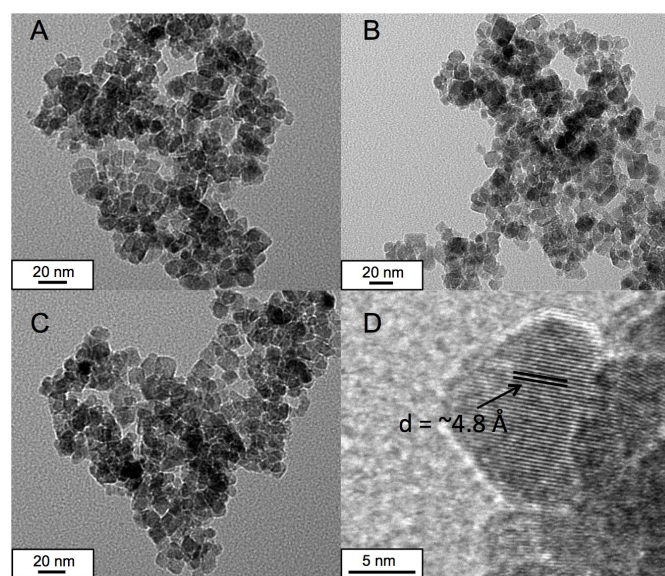


Figure 3: TEM images of **IONBsX100**.

We acknowledge the difficulty in precisely distinguishing between octahedral and rhombohedral shapes based on the 2D information provided by TEM. It is possible that solely one or the other shape is formed exclusively, or even a mixture. Figures 5A and 5B show HR-TEM images of **IONBsX45** and **IONBsX100**, respectively, and Figure 5C shows a 3D representation of an octahedron for comparison.

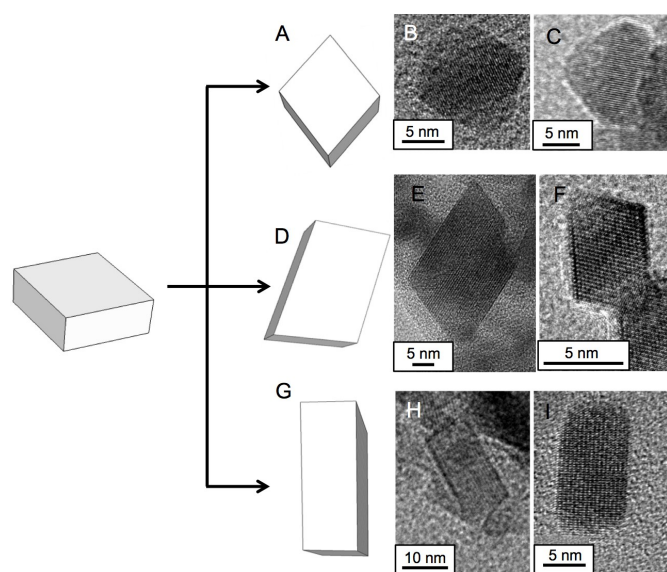


Figure 4: Comparison between a representative polyhedral brick-like shape with how it may appear with changes to size and viewing position. Image A shows this rhombohedral shape as seen perpendicular to its face, while B and C show HR-TEM images of this for **IONBsX45** and **IONBsX100**, respectively. Elongation along one edge leads to a parallelepiped as in image D. HR-TEM images of this shape for **IONBsX45** are shown in figures E and F. The same shape as D seen along an edge leads to a purely rectangular shape, as in figure G. HR-TEM images H and I show examples of this shape seen in **IONBsX45**.

Other researchers, having synthesized IONPs showing similar shape profiles under TEM, have concluded that their particles are octahedral in shape.¹⁴ However, the existence of the larger rectangular and parallelepipedal shaped particles in our synthesis suggests that the rhombohedral shape is more likely. Mesoscale assembly – in which small particles fuse together through alignment of their crystal facets to produce larger particles – is one mechanism through which different particle shapes can be obtained.²⁴ Octahedral particles could not fuse together to form these kinds of shapes. On the other hand, if two rhombohedral particles fuse together in this manner they would result in a parallelepipedal shape. Figure 5D shows a schematic representation of this mechanism, and Figure 5E shows a TEM image of these two types of particles side by side. Examples of images taken with TEM at various tilt angles in order to visualize the effect of sight angle on the apparent shape of a particle are shown in the electronic supplementary information (see Figures S3 and S4, ESI[†]).

The used Triton X surfactants form LLC phases in water (see Figure S1, ESI[†], for textures under POM), and, through the formation of these phases, have been used as templates in nanomaterial synthesis. The formation of discrete, layered structures could contribute to the shape control seen here by constraining the direction of growth during particle formation. Other than templating, most shape control in nanomaterials results from control over material growth rate and precursor concentration (i.e. selective access to precursor atoms or monomers through local concentration gradients). In general this is accomplished through some combination of variation in heating rate and the overall temperature of the reaction

medium, as well as the use of selective capping agents, which preferentially adsorb onto certain crystal facets.²⁵ Our

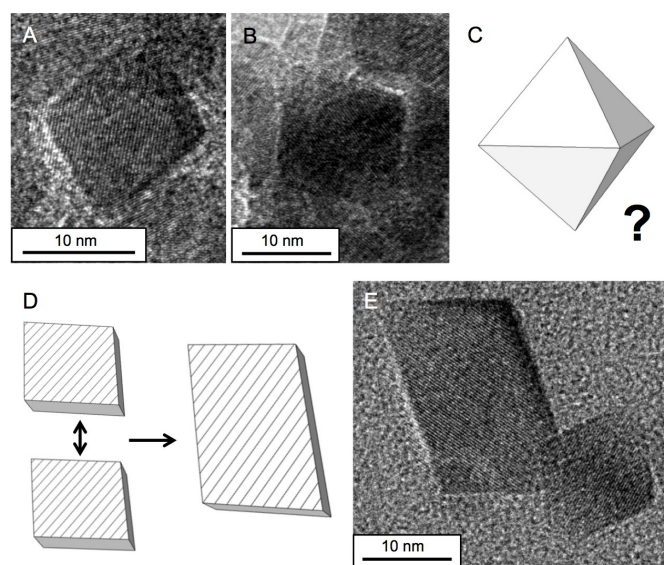


Figure 5: Visualization of the discussion on the possibility of octahedral vs. rhombohedral shapes. Figures 5A and 5B show HR-TEM images of particles from **IONBsX45**. Similar images can be seen in other syntheses which conclude these are octahedral particles (as in image C). Figure 5D shows how two rhombohedral particles could fuse *via* mesoscale assembly to form one larger polyhedral particle. Figure 5E shows a TEM image of these two types of particle shapes side by side from **IONBsX45**.

modified co-precipitation method requires a much lower reaction temperature than methods using adjusted heating rate and temperature as means of shape control. However, the surfactant molecules may be acting as capping agents. Changes in the nature of capping agent functional groups (i.e. the presence or absence of certain functional groups as well as changes in the ratio between different capping agents) can lead to changes in IONP morphology.²⁶ Triton X45 and X100 have similar structures, differing only in the length of the ethylene oxide chain. Variations in the chain length of capping agents have been shown to influence shape in other metal oxide particles; the longer PEO chain length of the X100 molecule could account for the restriction in diversity of the resulting particle shapes. The longer X100 chain could also prevent smaller particles from coming close enough together to fuse and form larger particles *via* mesoscale assembly, which would account for the absence of larger parallelepipedal and rectangular particles in the synthesis of **IONBsX100**. Given the speed of the hydrolysis reaction and the dynamic nature of the reaction medium, all of the above mechanisms may contribute to the final particle shapes.

Magnetic measurements

Saturation magnetization (M_s) values were found to be 58 and 61 emu/g at 300 K for **IONBsX45** and **IONBsX100**, respectively. These values are typical of crystalline IONPs on the order of tens of nanometers in size.²⁷ Both types of particles were found to have low coercivity (H_c) values of 18 and 20 Oe

for IONBsX45 and IONBsX100, respectively. These results are shown in Figure 6.

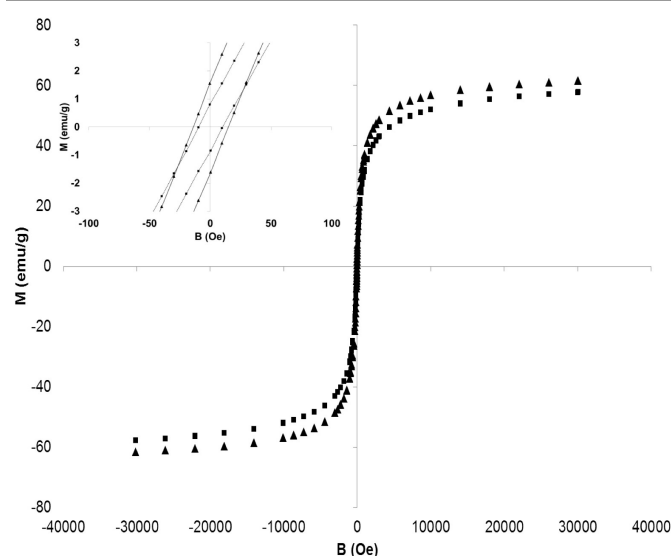


Figure 6: Magnetic hysteresis curves for IONBsX100 (triangles) and IONBsX45 (squares) at 300 K. Inset shows a magnified image of the coercivity for each particle set.

Surface functionalization and characterization

One of the many benefits of an aqueous synthesis is the ease with which particles can be coated with hydrophilic functional groups. In the present case, the IONBs, free of any surfactant from the initial synthesis (Figure S6, ESI[†]), were coated with *N*-(trimethoxysilylpropyl)ethylenediaminetriacetate trisodium salt (EDTS) through injection of the silane solution directly into the reaction media after the synthesis. Particles coated with the above siloxane are labelled *S*-IONBsX. EDTS can impart a high negative surface potential on the particles, which allows them to be easily stabilized in aqueous media. Additionally, previous investigations on the cell viability and uptake properties of EDTS-coated spherical IONPs have demonstrated the usefulness of this molecule as a functionalizing agent for IONPs in bioapplications.²⁸ The dried particles were analyzed by TEM to corroborate the formation of nanobrick shapes as well as FT-IR and TGA to confirm the presence and binding of the EDTS surface coating (see Figures S2 and S8, ESI[†]). The dried particles could be re-suspended in water with mild sonication, and remained stable for weeks without any sign of precipitation.

Table 1: Physicochemical properties of silanized particles in water.

Material	DLS (nm)	ζ -potential (mV)	pH
<i>S</i> -IONBsX45	50.9 ± 1.4	-44.2 ± 2.4	9.8
<i>S</i> -IONBsX100	64.0 ± 0.4	-38.1 ± 1.0	9.4
<i>S</i> -IONPs	30.3 ± 1.0	-36.8 ± 2.8	10.2

Characterization of the particle suspensions was done with dynamic light scattering (DLS) and ζ -potential measurements.

Figure 7 shows a set of images of *S*-IONBsX45 suspended in water, and a summary of their properties in solution can be found in Table 1 (see also Figure S5, ESI[†]). For comparison, quasi-spherical IONPs were synthesized and coated with the same siloxane, following a previous report.²⁹ These particles are labelled *S*-IONPs. It should be noted that while the particles were added to distilled water rather than a buffer, the pH of the media was basic due to the nature of the surface coating itself (which contains the conjugate base of a carboxylic acid). Both particle size and surface potential when in solution are highly dependent on pH, as well as ionic strength, which may explain the slight differences between the X45 and X100 particles. These particle dispersions were then used for both MRI relaxivity and hyperthermia measurements described below.

MRI relaxivity measurements

The transverse (r_2) and longitudinal (r_1) relaxivities of *S*-IONBsX45 and *S*-IONBsX100 are shown in Table 2 (see Figure S7 in ESI[†] for relaxation time vs. Fe concentration plots used to calculate r_2 and r_1). The properties of quasi-spherical *S*-IONPs were also measured for comparison. Table 2 lists results at 1.5 T and 7 T. The r_1 values for the three particle types are low and roughly similar. Since iron oxide materials are not typically considered viable T_1 contrast agents, this is unsurprising. The r_2 values of both types of anisometric particle systems are an order of magnitude higher than the spherical IONPs, however. This is true at both 1.5 and 7 T field strengths. The ratio of r_2/r_1 – which is a measure of the efficiency of the contrast agent, where a low ratio is favorable for T_1 agents, and a high ratio is favorable for T_2 agents – is also shown. These results demonstrate that the polyhedral NBs are much more efficient T_2 contrast agents as compared with the spherical NPs coated with the same surface ligands.

Table 2: Relaxivity values at different field strengths for EDTS coated particles.

	@ 1.5 T			@ 7 T		
	r_1 (mM ⁻¹ s ⁻¹)	r_2 (mM ⁻¹ s ⁻¹)	r_2/r_1	r_1 (mM ⁻¹ s ⁻¹)	r_2 (mM ⁻¹ s ⁻¹)	r_2/r_1
<i>S</i> -IONPs	8.8	29.6	3.4	2.5	43.9	17.7
<i>S</i> -IONBsX45	12.2	285	23.4	1.4	423	298
<i>S</i> -IONBsX100	11.8	247	21.0	4.3	599	139

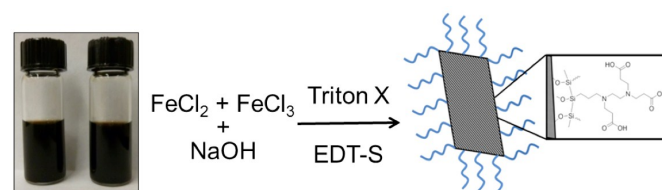


Figure 7: (Left): Picture of particle dispersions of *S*-IONBsX45 and *S*-IONBsX100. (Right): Schematic representation of the reaction scheme resulting in coated brick-like particles.

Table 3 shows the relaxivity properties of selected iron oxide based contrast agents reported in the literature, both commercial and otherwise. Feridex and Combidex are two types of commercial IONP-based contrast agents, often used for baseline comparison. Their specific properties vary depending upon the literature cited (two examples are given), but in all cases both **S-IONB** systems show an order of magnitude higher r_2 and r_2/r_1 values.

MPIOs (micrometer-sized iron oxide particles), aggregates of nanometer sized IONPs, have been shown to increase the r_2 value as compared with dispersions of non-aggregated particles. Even still, our polyhedral particles have nearly double the r_2 value seen with MPIOs. Three other types of particles that do show higher r_2 values have been included as well.

FIONs (ferrimagnetic iron oxide nanocubes) have a reported r_2 value of $324 \text{ mM}^{-1} \text{ s}^{-1}$ measured at 1.5 T; VNPs (virus-based nanoparticles) have a reported value of $140.28 \text{ mM}^{-1} \text{ s}^{-1}$, with a favorable r_2/r_1 value of 144.6, measured at 3 T; and octapod IONPs have a reported value of $679 \text{ mM}^{-1} \text{ s}^{-1}$ measured at 7 T. Each system contains highly anisometric particles, demonstrating the important effect that particle morphology has on their efficiency in MRI applications. In all above cases, particles were synthesized using variations on thermal decomposition methods. We contend that since the relaxivity values reported are not significantly different ($324 \text{ vs. } 285 \text{ mM}^{-1} \text{ s}^{-1}$ for FIONs *vs.* **S-IONBsX45**; $679 \text{ vs. } 599 \text{ mM}^{-1} \text{ s}^{-1}$ for octapod IONPs *vs.* **S-IONBsX100**), the benefits associated with our synthesis allow our particles to be viable alternatives.

Table 3: Comparison between commercially available and literature reported iron oxide based contrast agents.

	r_2 ($\text{mM}^{-1} \text{ s}^{-1}$)	r_2/r_1	Field strength	references
Feridex	41, 98.3	8.7, 4.1	1.5 T	30, 31
Resovist	61, 151	7.1, 5.9	1.5 T	31, 32
MPIO	169	-	1.5 T	32
FION	324	-	1.5 T	32
VNPs	140.28	144.6	3 T	33
Octapod IONPs	679	-	7 T	34

Hyperthermia measurements

The hyperthermia performance of the **S-IONBs** was evaluated by exposing particle dispersions to an AC magnetic field on a custom instrument (described in a previous report).³⁵ The SLP (specific loss power, also often referred to as SAR, specific absorption rate) values of the samples were calculated in order to measure the efficiency of the particles at converting the magnetic field energy to heat with respect to the amount of iron in each sample. This was calculated using equation (1):

$$SLP = C m_s / m (\Delta T / \Delta t) \quad (1)$$

where C is the specific heat of the solution (taken to be the same as water, $4.186 \text{ J/g}^\circ\text{C}$), m_s is the mass of the solution, m is the mass of the magnetic material (in this case the mass of Fe,

established by ICP analysis), and $\Delta T / \Delta t$ is the slope of the heating curve. SLP values are highly dependent on the strength of the magnetic field, the nature of the media, how one chooses to evaluate the $\Delta T / \Delta t$ curve, and even the placement of the temperature probe.³⁶ As such, comparisons between materials used by different researchers with different experimental setups and protocols are problematic. In order to obtain an internal comparison the **IONBs** were compared with quasi-spherical **IONPs** to act as a kind of internal standard, as with the MRI relaxivity measurements. Figure 8 shows the temperature *vs.* time curves for the three types of particle dispersions measured, along with the calculated SLP values. The graphs clearly show that the quasi-spherical particles (**S-IONPs**) perform the worst, giving rise to a mere 2.6°C temperature change over 3 minutes, yielding an SLP value of 32.7 W/g . The **IONBs** show an order of magnitude more efficient heating response, with a 28.3°C temperature change and 166 W/g SLP value for **S-IONBsX100**, and a 29.2°C temperature change and a 415 W/g SLP value for **S-IONBsX45**.

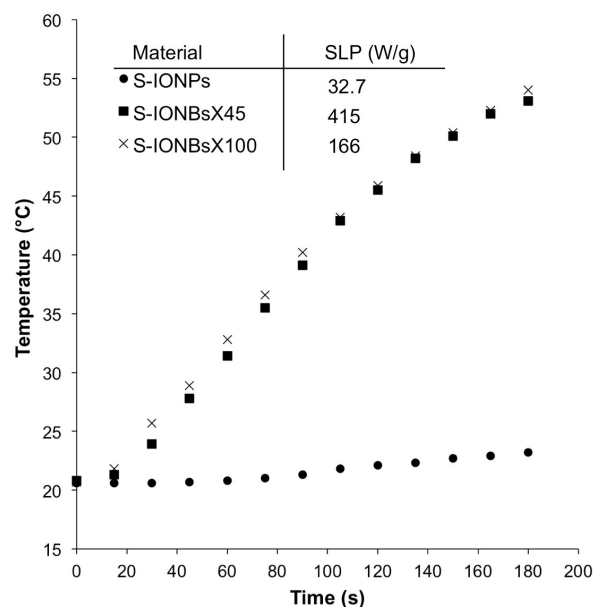


Figure 8: Increase in temperature *vs.* time for different particle dispersions during exposure to AC magnetic field. Inset: calculated SLP values for each set of particles. AC field was set at an amplitude of 20 kA/m, and a frequency of 2 MHz.

Previous reports have suggested that single crystalline particles on the order of 18 nm in size are the most efficient for hyperthermia applications. This may account for the low SLP value for the **S-IONPs**, which are $<10 \text{ nm}$ according to the literature. However, the same report suggests that low polydispersity in particle size yields greater efficiency. This should preclude higher SLP values for **S-IONBsX45** and **S-IONBsX100** given their high polydispersity due to the mixture of shapes produced. In the end, the complicated interplay between particle shape, surface anisotropy and overall size distribution may equally contribute to SLP values, which makes direct conclusions as to what accounts for the numbers seen here difficult. Further work in the isolation of particular shapes

from the mixtures produced will allow for a better understanding as to which properties contribute the most to high SLP values.

Conclusions

This study presents the synthesis of polyhedral particles of iron oxide *via* a modification of the aqueous co-precipitation method with Triton X surfactants. A variety of shapes – variations on cubic and rectangular “brick-like” shapes, deemed **IONBs** – are formed, with the precise mixture dependent on the surfactant used. The resulting particles are highly crystalline, and their surface properties can easily be modified with the *in situ* addition of a hydrophilic siloxane. Silanized **IONBs** remain stable when dispersed in water, allowing for applications in medicine. Their efficacy in two such applications, hyperthermia and MRI contrast, were investigated. Both types of particle systems, **S-IONBsX45** and **S-IONBsX100**, have SLP values an order of magnitude higher than spherical IONPs with the same siloxane coating. Additionally, both “nanobrick” systems show highly favorable MRI T_2 contrast properties, with r_2 values comparable to the highest reported in the literature. We have shown an effective alternative strategy for the control of IONP morphology that is simple, cost-effective, water-based, and also environmentally friendly. In addition, these particles have been investigated for their applications in cell uptake and for their potential as drug delivery vehicles. Recent studies by Sun *et al.* on **S-IONBsX45** have shown that these particles are taken up in endothelial cells at a rate far greater than spherical particles with the same surface coating and reasonably similar hydrodynamic radius and ζ -potential.³⁷ This demonstrates that IONP shape modification in general, and the specific shapes found in the particles discussed here, offer a potential means of targeted delivery to specific cells without the need for receptor-ligand interactions.

Experimental Section

Materials

Iron(II) chloride tetrahydrate (*Reagent Plus*, 98%), iron(III) chloride (reagent grade 97%), Triton X100 (laboratory grade), Triton X45, and sodium hydroxide (reagent grade, >98%) were purchased from Sigma-Aldrich. *N*-(trimethoxysilylpropyl) ethylenediaminetriacetate trisodium salt (45% in water) was purchased from Gelest Inc.

Transmission electron microscopy (TEM) imaging

TEM imaging was done with a FEI Tecnai TF20 TEM instrument at an accelerating voltage of 200 kV. Particle samples were dispersed in methanol and dropcast onto 400 mesh carbon coated copper grids.

XRD analysis

Powder X-ray diffraction patterns (XRD) were measured on an X'Pert PRO diffractometer manufactured by PANalytical, Inc.

(Westborough, MA, USA). The experimental setup used Bragg-Brentano geometry in θ - θ configuration, copper as a radiation source (Cu $K\alpha$ radiation), and a diffracted beam curved crystal monochromator to eliminate Cu $K\beta$. All patterns were collected in a range of 2θ values from 10.00° to 80.00° with a step size 0.05°.

MRI relaxivity measurements

The ionic relaxivity of the iron oxide particles was tested using a pre-clinical 7.0 T (300 MHz) MRI (Bruker BioSpec 70/30USR), and a Bruker Minispec mq60 relaxometer (60 MHz). A standard inversion recovery sequence protocol was used to determine the longitudinal T_1 values on each of the instruments. The transverse relaxivity (r_2) of the particles was calculated as the slope of $1/T_2$ against iron concentration. T_2 relaxation times were determined using a standard Carr-Purcell-Meiboom-Gill spin echo sequence.

Hyperthermia measurements

Dispersions of **S-IONBsX45** and **S-IONBsX100** were made by sonicating dried powder in deionized water (at concentrations of 9.88 and 9.95 mg/mL, respectively). A dispersion of **S-IONPs**, synthesized similarly to a previous report, was also made in this manner at a concentration of (10.01 mg/mL). In a typical hyperthermia experiment, 250 μ L of particle dispersion was added to a single well from a 96-well plate. The samples were exposed to a field with an amplitude of 20 kA/m and a frequency of 2.1 MHz for 3 minutes while the temperature of the sample media was monitored using a fiber optic temperature probe (Neoptix).

Dynamic light scattering (DLS) and ζ -potential measurements

The hydrodynamic radius and ζ -potential of the **S-IONBs** were determined using a Brookhaven Zetaplus ζ -potential-DLS measurement system. The instrument specifications include a 35 mW class 1 laser at 660 nm with a scattering angle of 90°. All dispersions were measured at a concentration of \sim 1 mg/mL. Results listed are an average of 3 consecutive measurements.

Polarized optical microscopy (POM) imaging

POM images were taken with an Olympus BX-53 equipped with a Linkam LTS420E heating/cooling stage.

FT-IR sample preparation

Surface functionalization was analyzed through FT-IR using KBr pellet techniques. Approximately 1 mg of dried particles were mixed with approximately 150 mg of KBr, which was then pressed into a pellet. The pellet was stored in a vacuum oven at 50 °C for several hours before analysis to remove any adsorbed water. Spectra were recorded using a Magna Nicolet-500 series FT-IR spectrometer.

Thermal Gravimetric Analysis (TGA) measurements

The amount of surface ligands on the particles was estimated *via* a TA instruments TGA Q500. The heating rate was set at 10 °C/min. Powdered samples were typically dried in a vacuum

oven at 50 °C for 2 hours before analysis in order to eliminate any surface water.

Magnetic Measurements

The magnetic properties were characterized with an RF Superconducting Quantum Interference Device (SQUID) magnetometer (Quantum Design MPMS-XL) with reciprocating sample transport. The field was applied between –30 to +30 kOe at 300 K.

Acknowledgments

M.W. would like to thank Michal Marszewski for his help obtaining the XRD spectra. M.A.B. would like to thank the NIH for the training grant T32 HL105338. N.F.S. would like to acknowledge the support of the National Science Foundation (NSF) grant CMMI NM 1333651. J.M.K. offers thanks for the NSF grant DMR-1206270. This work was also supported by the Ohio Third Frontier (OTF) program for Ohio Research Scholars “Research Cluster on Surfaces in Advanced Materials” (support for T.H.), which also supports the cryo-TEM facility at the Liquid Crystal Institute (KSU), where current TEM data were acquired. Finally, C.L. and T.H. would like to acknowledge funding for the NSF-REU Program (CHE-1263087).

Notes

†Electronic supplementary information (ESI) available: POM (polarized optical microscopy images), FT-IR, DLS, TGA, HR-TEM, and plots of MRI relaxation time vs. Fe concentration.

Author Affiliation

^a Department of Chemistry and Biochemistry, Kent State University, Kent, OH

^b Department of Biomedical Engineering, Case Western Reserve University, Cleveland, OH

^c Departments of Radiology, Materials Science and Engineering, and Macromolecular Science and Engineering, Case Western Reserve University, Cleveland, OH

^d Department of Biological Sciences, Kent State University, Kent, OH

^e Department of Physics & Astronomy, University of Pennsylvania, Philadelphia, PA

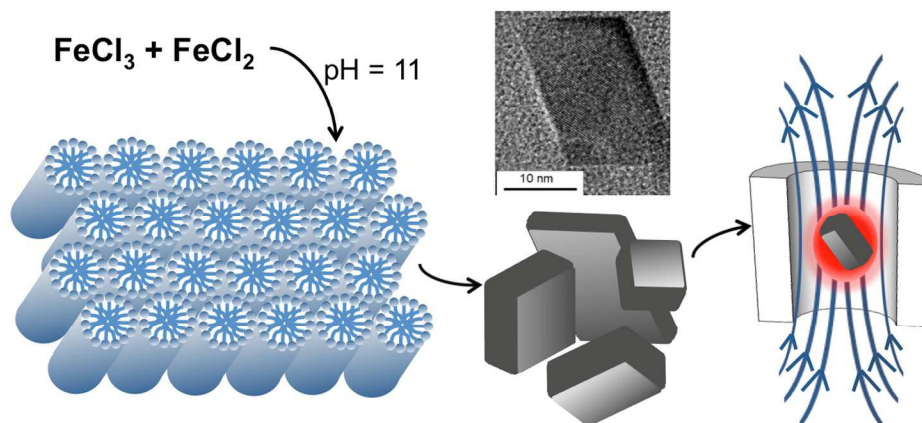
^f Liquid Crystal Institute, Chemical Physics Interdisciplinary Program, Kent State University, Kent, OH

References

- 1 H. Parham, B. Zargar and R. Shiralipour, *J. Hazard. Mater.*, **2012**, 205–206(0), 94–100.
- 2 Q. Qu, S. Yang and X. Feng, *Adv. Mater.*, **2011**, 23(46), 5574–5580.
- 3 H. Firouzabadi, N. Iranpoor, M. Gholinejad and J. Hoseini, *Adv. Synth. Cat.*, **2011**, 353(1), 125–132.
- 4 a) J. Guo, W. Yang and C. Wang, *Adv. Mater.*, **2013**, 25(37), 5196–5214. b) E. Amstad, M. Textor and E. Reimhult, *Nanoscale*, **2011**(7), 2819–2843. c) R. Qiao, C. Yang and M. Gao, *J. Mater. Chem.*, **2009**, 19(35), 6274–6293.
- 5 R. Massart, *IEEE Trans. Magn.*, **1981**, 17(2), 1247–1248.
- 6 V. Yathindranath, L. Rebbouh, D. F. Moore, D. W. Miller, J. van Lierop and T. Hegmann, *Adv. Funct. Mater.*, **2011**, 21(8), 1457–1464.
- 7 S. Sun, H. Zeng, *J. Am. Chem. Soc.*, **2002**, 124(28), 8204–8205.
- 8 a) J. Park, K. An, Y. Hwang, J. Park, H. Noh, J. Kim, J. Park, N. Hwang and T. Hyeon, *Nat. Mater.*, **2004**, 3(12), 891–895. b) N. Pinna, S. Grancharov, P. Beato, P. Bonville, M. Antonietti and M. Niederberger, *Chem. Mater.*, **2005**, 17(11), 3044–3049. c) H. Liu, S. P. Ko, J. Wu, M. Jung, J. H. Min, J. H. Lee, B. H. An and Y. K. Kim, *J. Magn. Magn. Mater.*, **2007**, 310(2, Part 3), e815–e817.
- 9 C. Lee, H. Jeong, S. T. Lim, M. Sohn and D. W. Kim, *ACS Appl. Mater. Interfaces.*, **2010**, 2(3), 756–759.
- 10 H. Yang, T. Ogawa, D. Hasegawa and M. Takahashi, *J. Appl. Phys.*, **2008**, 103(7), 07D526–07D528.
- 11 P. Guardia, J. Perez-Juste, A. Labarta, X. Batlle and L. M. Liz-Marzan, *Chem. Comm.*, **2010**, (33), 6108.
- 12 S. Palchoudhury, W. An, Y. Xu, Y. Qin, Z. Zhang, N. Chopra, R. A. Holler, C. H. Turner and Y. Bao, *Nano Lett.*, **2011**, 11(3), 1141–1146.
- 13 L. Bao, W. Low, J. Jiang and J. Y. Ying, *J. Mater. Chem.* **2012**, 22(15), 7117–7120.
- 14 A. Mitra, J. Mohapatra, S. S. Meena, C. V. Tomy and M. Aslam, *J. Phys. Chem. C*, **2014**, 118(33), 19356–19362.
- 15 R. De Palma, S. Peeters, M. J. Van Bael, d. R. Van, K. Bonroy, W. Laureyn, J. Mullens, G. Borghs and G. Maes, *Chem. Mater.* **2007**, 19(7), 1821–1831.
- 16 N. R. Jana, C. Earhart and J. Y. Ying, *Chem. Mater.* **2007**, 19(21), 5074–5082.
- 17 V. Yathindranath, V. Ganesh, M. Worden, M. Inokuchi and T. Hegmann, *RSC Adv.*, **2013**(24), 9210–9213.
- 18 C. Fritscher, N. Husing, S. Bernstorff, D. Brandhuber, T. Koch, S. Seidler and H. C. Lichtenecker, *J. Synchrotron Rad.* **2005**, 12(6), 717–720.
- 19 S. V. Ahir, P. G. Petrov and E. M. Terentjev, *Langmuir*, **2002**, 18(24), 9140–9148.
- 20 M. Kim, I. Yamayoshi, S. Mathew, H. Lin, J. Nayfach and S. Simon, *Ann. Biomed. Eng.* **2013**, 41(3), 598–609.
- 21 R. Hergt, S. Dutz, R. Müller and M. Zeisberger, *J. Phys.: Condens. Matter.*, **2006**, 18(38), S2919–S2934.
- 22 H. B. Na, I. C. Song and T. Hyeon, *Adv. Mater.*, **2009**, 21(21), 2133–2148.
- 23 E. D. Smolensky, H. E. Park, Y. Zhou, G. A. Rolla, M. Marjanska, M. Botta and V. C. Pierre, *J. Mater. Chem. B.*, **2013**, 1(22), 2818–2828.
- 24 Q. Zhang, S. Liu and S. Yu, *J. Mater. Chem.*, **2009**, 19(2), 191–207.
- 25 T. Nguyen, *Nanoscale*, **2013**, 5(20), 9455–9482.
- 26 A. Shavel, B. Rodríguez-González, J. Pacifico, M. Spasova, M. Farle and L. M. Liz-Marzán, *Chem. Mater.*, **2009**, 21(7), 1326–1332.
- 27 G. F. Goya, T. S. Berquo, F. C. Fonseca, and M. P. Morales, *J. Appl. Phys.*, **2003**, 94(5), 3520–3528.

- 28 Z. Sun, M. Worden, Y. Wroczynskyj, V. Yathindranath, J. van Lierop, T. Hegmann, and D. W. Miller, *Int. J. Nanomed.*, **2014**, *9*, 3013-3026.
- 29 V. Yathindranath, Z. Sun, M. Worden, L. J. Donald, J. A. Thliveris, D. W. Miller and T. Hegmann, *Langmuir*, **2013**, *29*(34), 10850-10858.
- 30 M. Rohrer, H. Bauer, J. Mintorovitch, M. Requardt and H. Weinmann, *Invest. Radiol.*, **2005**, *40*(11), 715-24.
- 31 Y. Wang, *Quant. Imaging Med. and Surg.*, **2011**, *1*(1), 35-40.
- 32 N. Lee, H. Kim, S. H. Choi, M. Park, D. Kim, H. Kim, Y. Choi, S. Lin, B. H. Kim, H. S. Jung, H. Kim, K. S. Park, W. K. Moon and T. Hyeon, *Proc. Natl. Acad. Sci. U. S. A.*, **2011**, *108*(7), 2662-2667.
- 33 X. Huang, B. D. Stein, H. Cheng, A. Malyutin, I. B. Tsvetkova, D. V. Baxter, N. B. Remmes, J. Verchot, C. Kao, L. M. Bronstein and B. Dragnea, *ACS Nano*, **2011**, *5* (5), 4037-4045.
- 34 Z. Zhao, Z. Zhou, J. Bao, Z. Wang, J. Hu, X. Chi, K. Ni, R. Wang, X. Chen, Z. Chen and J. Gao, *Nature Comm.*, **2013**, *4*, 2266.
- 35 M. Kim, I. Yamayoshi, S. Mathew, H. Lin, J. Nayfach and S. Simon, *Ann. Biomed. Eng.*, **2013**, *41*(3), 598-609.
- 36 Shu-Yi Wang, Shujuan Huang and D. Borca-Tasciuc, *IEEE Trans. Magn.*, **2013**, *49*(1), 255-262.
- 37 Z. Sun, M. Worden, Y. Wroczynskyj, J. A. Thliveris, J. van Lierop, T. Hegmann and D. W. Miller. "Differential internalization of brick shaped iron oxide nanoparticles by endothelial cells," submitted to *Nano Today*.

TOC entry:



Iron oxide nanobricks prepared by co-precipitation in lyotropic liquid crystal phases are versatile and effective theranostic materials for magnetic hyperthermia, T_2 MRI contrast enhancement and differential cell internalization.